

# Rapid and accurate estimation of blood saturation, melanin content, and epidermis thickness from spectral diffuse reflectance

Dmitry Yudovsky and Laurent Pilon\*

University of California, Los Angeles, Henri Samueli School of Engineering and Applied Science,  
Mechanical and Aerospace Engineering Department, Biomedical Inter-Department Program,  
Los Angeles, California 90095-1597, USA

\*Corresponding author: pilon@seas.ucla.edu

Received 13 November 2009; revised 25 February 2010; accepted 1 March 2010;  
posted 4 March 2010 (Doc. ID 119962); published 22 March 2010

We present a method to determine chromophore concentrations, blood saturation, and epidermal thickness of human skin from diffuse reflectance spectra. Human skin was approximated as a plane-parallel slab of variable thickness supported by a semi-infinite layer corresponding to the epidermis and dermis, respectively. The absorption coefficient was modeled as a function of melanin content for the epidermis and blood content and oxygen saturation for the dermis. The scattering coefficient and refractive index of each layer were found in the literature. Diffuse reflectance spectra between 490 and 620 nm were generated using Monte Carlo simulations for a wide range of melanosome volume fraction, epidermal thickness, blood volume, and oxygen saturation. Then, an inverse method was developed to retrieve these physiologically meaningful parameters from the simulated diffuse reflectance spectra of skin. A previously developed accurate and efficient semiempirical model for diffuse reflectance of two layered media was used instead of time-consuming Monte Carlo simulations. All parameters could be estimated with relative root-mean-squared error of less than 5% for (i) melanosome volume fraction ranging from 1% to 8%, (ii) epidermal thickness from 20 to 150  $\mu\text{m}$ , (iii) oxygen saturation from 25% to 100%, (iv) blood volume from 1.2% to 10%, and (v) tissue scattering coefficient typical of human skin in the visible part of the spectrum. A similar approach could be extended to other two-layer absorbing and scattering systems. © 2010 Optical Society of America

OCIS codes: 100.3190, 170.1470, 170.1870, 170.3660, 170.3880, 170.6510.

## 1. Introduction

Diffuse reflectance spectroscopy has found many applications in noninvasive monitoring of biological tissues [1–7]. This technique investigates tissue structure, chromophore concentration, and health by measuring the tissue's optical properties. Commercially available devices typically analyze experimental data using the modified Beer–Lambert law to determine the relative concentrations of tissue chromophores, such as melanin, blood, water, or hemoglobin, in arbitrary units [6,8–13]. However, the tissue

scattering coefficient cannot be retrieved [10,14]. Alternatively, diffuse reflectance data processed with the diffusion approximation [15] can yield absolute chromophore concentration and measure the tissue's scattering coefficient [16], which is related to tissue microstructure [16–19]. However, this technique requires emitter–detector separation of up to 1 cm, thus limiting the spatial resolution of these devices [20,21].

Current spectroscopic techniques are based on the assumption that tissue is homogeneous and that properties are independent of depth [6,7,9,11,22,23]. In reality, most bodily organs, such as skin, the intestine, or the cervix, are protected by a thin lining called the epithelial layer [24]. While the organ is

typically composed of connective tissues and perfused with blood vessels and nerves, the protective epithelial layer is bloodless and consists of structured cell layers [24]. Differences in cellular structure and chemical composition give rise to distinct optical properties, making the assumption of tissue homogeneity questionable [25]. In skin, for example, the outer epidermal layer is pigmented by melanin, which absorbs strongly in the UV, while the inner dermal layer is pigmented by blood, which absorbs in the visible and near-infrared parts of the spectrum [26]. Furthermore, the thickness of the epidermal layer may vary with anatomical location, gender, and age [27–29].

Multilayer optical models of tissue have been developed [13,30–32] to study the effects of tissue structure and chromophore distribution on light propagation. However, such models are computationally intensive and cannot be used in real-time clinical applications [33]. Semiempirical models of light transfer have been developed to accelerate computation without significant loss of accuracy [34–38]. Mantis and Zonios [34], for example, developed a semiempirical model for diffuse reflectance of two-layer media. They used their model in an inverse method to determine the optical properties of two-layer tissue phantoms of variable epithelial thickness. However, their method requires that the bottom layer be scattering but nonabsorbing [34], which is not the case for most organs [24,26]. In addition, Tsumura *et al.* [36] developed a semiempirical model for diffuse reflectance of two-layer scattering and absorbing media based on the modified Beer–Lambert law. The authors assumed that the thickness of the top layer was equal to  $70\ \mu\text{m}$  [36]. Recently, Yudovsky and Pilon [35] developed a semiempirical model that predicts the diffuse reflectance of strongly scattering two-layer media. The model accounted for (i) absorption and anisotropic scattering in both layers, (ii) variable thickness of the top layer, and (iii) internal reflection at the medium/air interface. It was shown to accurately predict the diffuse reflectance of skin [35].

The objective of this study is to develop an inverse method based on our semiempirical model [35] and to assess its robustness in estimating the scattering coefficients, chromophore concentrations in both epidermis and dermis, and the epidermal thickness from spectral diffuse reflectance of human skin.

## 2. Background

### A. Human Skin

Skin is the largest organ of the human body, representing a total surface area of approximately  $1.8\ \text{m}^2$  and a total weight of approximately 11 kg for adults [39]. The epidermis and dermis are the two main layers. They are separated by the basement membrane and rest on the subcutaneous fat layer [39]. The topmost layer of the epidermis is called the stratum corneum and is composed of dead cells embedded in a lipid matrix. The rest of the epidermis

is mainly composed of keratinocytes, melanocytes, and langerhans [39]. Melanocytes synthesize melanin, the skin protein mainly responsible for skin color. Melanin is contained in organelles known as melanosomes, which are distributed throughout the epidermis [39]. Depending on genetic factors and UV light exposure, melanosomes occupy 1% to 43% of the epidermal volume, corresponding to light or dark pigmented skin, respectively [40–42]. Epidermal thickness varies with bodily location and ranges between 20 and  $150\ \mu\text{m}$  [26,42–44].

The dermis, located beneath the epidermis, is responsible for the skin's pliability, mechanical resistance, and temperature control. It contains touch, pressure, and temperature receptors, as well as sebaceous and sweat glands and hair follicles [39]. The dermis is composed of collagen fibers perfused by nerves, capillaries, and blood vessels [26,45,46]. The thickness of the dermis ranges between 450 and  $650\ \mu\text{m}$  [27,47]. Depending on body location and tissue health, the volume of blood in the dermis ranges between 0.2% and 7% [42,48,49]. Approximately half of the blood volume is occupied by erythrocytes (red blood cells), which are responsible for oxygen transfer from the lungs to the rest of the body [42,49]. Erythrocytes are composed mainly of hemoglobin molecules, which reversibly bind to oxygen molecules in the lungs to form oxyhemoglobin. Hemoglobin is known as deoxyhemoglobin once it has released its oxygen molecules. The ratio of oxyhemoglobin molecules to the total number of hemoglobin molecules in the blood is the so-called oxygen saturation denoted by  $\text{SO}_2$ . Hemoglobin absorption dominates the total absorption of the dermis in the visible range [26,39,46]. Furthermore, the spectral extinction coefficient of oxyhemoglobin differs significantly from that of deoxyhemoglobin. Thus, the color of the dermis depends on the average oxygen saturation of its blood content.

### B. Skin Properties Measurement

Various techniques exist to measure chromophore concentrations and blood saturation of human skin. Commercially available noninvasive, optical devices typically measure these quantities in a small region of 1 to 2 cm in diameter and report a device specific melanin (MI) and erythema (EI) index [40,50]. The MI corresponds qualitatively to the darkness of skin, while EI corresponds to the redness or inflammation of skin. Such devices have been used to predict the risk of melanoma skin cancer [40] and as dosimetry feedback during laser treatment of port-wine stains [51] and acne [52]. Recently, hyperspectral imaging in the visible and near-infrared parts of the spectrum has been used to determine the spatial distribution of oxygen saturation in the human skin [12]. This technique has been applied clinically to study diabetic neuropathy [53] and predict the healing potential of diabetic foot ulcers [4,54]. Such devices typically assume a homogeneous tissue structure and do not model changes in the scattering coefficient

with wavelength or biological state, or from patient to patient. Thus, only relative chromophore concentration in arbitrary units can be reported [10,12,13]. Furthermore, epidermal thickness and blood volume cannot be determined [10].

Epidermal thickness varies naturally with age, gender, and body location [27–29,55]. It may also increase or decrease due to external stimuli. For example, UV exposure of human skin has been shown to increase the thickness of the epidermis in addition to increasing its melanin content [56,57]. On the other hand, smoking has been shown to decrease epidermal thickness [55]. Epidermal thickness can be measured reliably with punch biopsy, whereby a sample of the skin is removed and analyzed *ex vivo* [27,55,57]. This invasive technique can be painful and destroys the sample. Alternatively, noninvasive measurements of epidermal thickness can be made with techniques including optical coherent tomography or ultrasound [58,59]. However, these techniques are primarily sensitive to the tissue's scattering coefficient; therefore, simultaneous determination of chromophore concentration is difficult [60,61].

### C. Radiative Transfer Equation

Biological tissues, such as skin, are generally absorbing and strongly scattering media [33]. Light transfer through such turbid media is governed by the radiative transfer equation (RTE), written as [15]

$$\hat{s} \cdot \nabla I(\hat{r}, \hat{s}, \lambda) = -\mu_a(\lambda)I(\hat{r}, \hat{s}, \lambda) - \mu_s(\lambda)I(\hat{r}, \hat{s}, \lambda) + \frac{\mu_s(\lambda)}{4\pi} \int_{4\pi} I(\hat{r}, \hat{s}_i, \lambda) \Phi(\hat{s}_i, \hat{s}, \lambda) d\Omega_i, \quad (1)$$

where  $I(\hat{r}, \hat{s}, \lambda)$  is the spectral intensity at location  $\hat{r}$  in a unit solid angle  $d\Omega$  around direction  $\hat{s}$  expressed in  $W/cm^2 \cdot sr \cdot nm$ . The linear spectral absorption and scattering coefficients are denoted by  $\mu_a(\lambda)$  and  $\mu_s(\lambda)$ , respectively, and are expressed in  $cm^{-1}$ , while the scattering phase function is denoted by  $\Phi(\hat{s}_i, \hat{s}, \lambda)$ . The Henyey–Greenstein scattering phase function is an approximate expression that accounts for the anisotropic nature of scattering and is given by [62]

$$\Phi(\hat{s}_i, \hat{s}, \lambda) = \frac{1 - g(\lambda)}{[1 + g(\lambda)^2 - 2g(\lambda) \cos \Theta]^{3/2}}, \quad (2)$$

where  $\Theta$  is the angle between  $\hat{s}$  and  $\hat{s}_i$  and  $g(\lambda)$  is the Henyey–Greenstein asymmetry factor used extensively in tissue optics [33,63,64]. The values of  $g(\lambda)$  measured for the epidermis and dermis were approximately the same and range between 0.73 and 0.82 in the visible range [46]. To account for the magnitude and anisotropy of the scattering phenomenon, the transport single scattering albedo  $\omega_{tr}(\lambda)$  is defined as [15]

$$\omega_{tr}(\lambda) = \frac{\mu_{s,tr}(\lambda)}{\mu_{s,tr}(\lambda) + \mu_a(\lambda)} = \frac{\mu_s(\lambda)[1 - g(\lambda)]}{\mu_s(\lambda)[1 - g(\lambda)] + \mu_a(\lambda)}, \quad (3)$$

where  $\mu_{s,tr}(\lambda) = \mu_s(\lambda)[1 - g(\lambda)]$  is the transport scattering coefficient.

Monte Carlo simulation is a stochastic method for solving differential equations, such as the RTE [15,32], and has been applied to study light transfer in skin [23,31,37,65]. To do so, a stochastic model is constructed such that the expected value of a certain random variable is equivalent to the value of a physical quantity that is determined by the exact differential equation [66]. The expected value is estimated by sampling the random variable multiple times. In effect, by repeating the simulation, the variance of the estimate diminishes. Thus, albeit at the cost of time, the solution may be found with arbitrary accuracy by increasing the number of simulations [32,66].

### D. Semiempirical Model of Diffuse Reflectance

Recently, Yudovsky and Pilon [35] developed an approximate expression for the diffuse reflectance of skin treated as a two-layer media and given by

$$R_e = R^*[R_-(n_1, \omega_{tr,epi}) - R_-(n_1, \omega_{tr,derm})] + R_-(n_1, \omega_{tr,derm}), \quad (4)$$

where  $\omega_{tr,epi}$  and  $\omega_{tr,derm}$  are the transport single scattering albedos of the epidermis and dermis, respectively, while  $n_1$  is the index of refraction of both layers. The reduced reflectance  $R^*$  is a function of a single semiempirical parameter  $\alpha$  and is expressed as [35]

$$R^* = \frac{\tanh(Y_{epi})}{1/\alpha + (1 - 1/\alpha) \tanh(Y_{epi})}. \quad (5)$$

The parameter  $Y_{epi}$  is the modified optical thickness, defined as  $Y_{epi} = \zeta(\mu_{a,epi} + \mu_{s,tr})L_{epi}$ , where  $L_{epi}$  is the physical thickness of the epidermis [67]. The parameter  $\zeta$  was approximated by a third-order polynomial [35]:

$$\zeta^2 = \frac{47}{52} + \frac{31}{49} \omega_{tr,epi} - \frac{49}{54} \omega_{tr,epi}^2 - \frac{17}{27} \omega_{tr,epi}^3. \quad (6)$$

Similarly, assuming the refractive index of tissue to be  $n_1 = 1.44$ , the semiempirical parameter  $\alpha$  was found to be [35]

$$1/\alpha = -0.569\omega_{tr,derm}^2 - 0.055\omega_{tr,derm} + 0.993. \quad (7)$$

The function  $R_-(n_1, \omega_{tr})$  appearing in Eq. (4) is the diffuse reflectance of a semi-infinite homogeneous layer, with transport single scattering albedo  $\omega_{tr}$  and index of refraction  $n_1$  given by [35]

$$R_-(n_1, \omega_{tr}) = [1 - \rho_{01}(n_1)][1 - \hat{\rho}_{10}(n_1, \omega_{tr})] \times \frac{\hat{R}_d(\omega_{tr})}{1 - \hat{\rho}_{10}(n_1, \omega_{tr})\hat{R}_d(\omega_{tr})}, \quad (8)$$

where  $\rho_{01}(n_1)$  is the normal-normal reflectivity of the tissue/air interface, defined as,

$$\rho_{01}(n_1) = \left( \frac{n_1 - n_0}{n_1 + n_0} \right)^2. \quad (9)$$

Expressions for  $\hat{\rho}_{10}$  and  $\hat{R}_d$  were given in Eqs. (26) and (27) of Ref. [35], respectively. The relative error between the semiempirical model and Monte Carlo simulations was typically around 3% and never more than 8% for the optical properties of skin in the visible [35].

### 3. Methods

#### A. Assumptions

Figure 1 shows the two-layer medium considered to approximate skin structure. It consisted of a plane-parallel slab of thickness  $L_{\text{epi}}$  representing the epidermis characterized by  $\mu_{a,\text{epi}}(\lambda)$  and  $\mu_{s,\text{tr}}(\lambda)$  and index of refraction  $n_1$ . This top layer was supported by a semi-infinite sublayer representing the dermis and characterized by  $\mu_{a,\text{derm}}(\lambda)$ ,  $\mu_{s,\text{tr}}(\lambda)$ , and  $n_2$ . The indices of refraction of both layers were assumed to be identical and constant with wavelength and depth (i.e.,  $n_1 = n_2$ ) [63]. The physical distance from the surface was denoted  $z$ . The thickness of epidermis  $L_{\text{epi}}$  was considered between 20 and 150  $\mu\text{m}$ . The incident light source was modeled as a collimated, monochromatic, and normally incident beam of infinite radius and intensity  $I_0(\lambda) = q_0(\lambda)\delta(\theta)$ . The quantity  $q_0(\lambda)$  denotes the radiative flux of the collimated beam and  $\delta(\theta)$  is the Dirac delta function. The air/epidermis interface and the interface between the slab and the semi-infinite sublayer were assumed to be optically smooth and, therefore, specularly reflecting. Then, radiative transfer can be considered as one dimensional [15,68]. Thus, the local intensity depends only on depth  $z$  and angle  $\theta$ , i.e.,  $I(\hat{\mathbf{r}}, \hat{\mathbf{s}}, \lambda) = I(z, \theta, \lambda)$  [15].

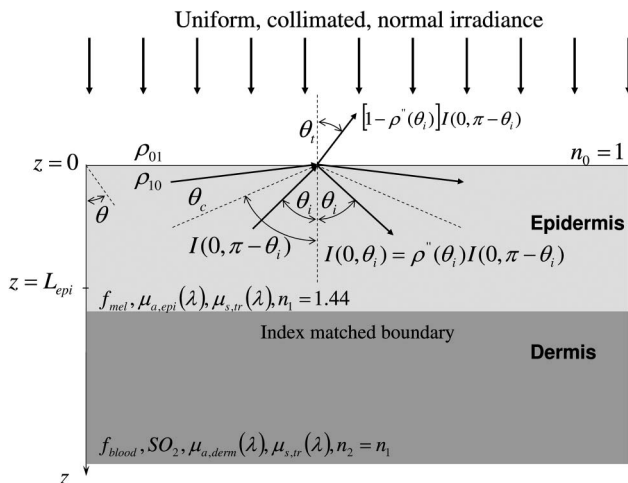


Fig. 1. Simplified skin geometry, biological properties, and optical characteristics of the epidermis and dermis considered in this study.

#### B. Closure Laws

To solve the RTE along with the associated boundary conditions [35] using the Monte Carlo method [32], the radiation properties of both the epidermis and dermis must be specified on a spectral basis.

##### 1. Reduced Scattering Spectrum

The reduced scattering coefficients of the epidermis and dermis were assumed to be equal and are given by the power law [33]:

$$\mu_{s,\text{tr}}(\lambda) = C \left( \frac{\lambda}{\lambda_0} \right)^{-b}, \quad (10)$$

where  $\lambda_0 = 1 \text{ nm}$  was introduced to ensure consistency in units. This approximate relationship is based on analytical [19,69–72] and experimental [17,73,74] studies of scattering in biological media and has been used to model tissue scattering in the visible and near-infrared parts of the spectrum. It has been shown experimentally that  $C$  and  $b$  depend on the average size of the microscopic features, such as cells or connective tissue, responsible for light scattering in the skin [17,70].

##### 2. Epidermis

Absorption in the epidermis is mainly due to melanin and flesh. Thus, the absorption coefficient in the epidermal layer  $\mu_{a,\text{epi}}(\lambda)$  was expressed as [42]

$$\mu_{a,\text{epi}}(\lambda) = \mu_{a,\text{mel}}(\lambda)f_{\text{mel}} + \mu_{a,\text{back}}(\lambda)(1 - f_{\text{mel}}), \quad (11)$$

where  $f_{\text{mel}}$  is the volume fraction of melanosomes and  $\mu_{a,\text{back}}(\lambda)$  is the background absorption of human flesh given by [42,75]

$$\mu_{a,\text{back}}(\lambda) = 7.84 \times 10^8 \lambda^{-3.255}. \quad (12)$$

The absorption coefficient of melanosomes as a function of wavelength has been approximated as [76]

$$\mu_{a,\text{mel}}(\lambda) = 6.60 \times 10^{11} \lambda^{-3.33}, \quad (13)$$

where  $\lambda$  and  $\mu_{a,\text{mel}}(\lambda)$  are expressed in nanometers and  $\text{cm}^{-1}$ , respectively. Figure 2(a) shows  $\mu_{a,\text{back}}$  and  $\mu_{a,\text{mel}}$  predicted by Eqs. (12) and (13) as a function of wavelength between 450 and 700 nm. It illustrates that melanin absorption of UV light is much stronger than that of near-infrared light. Indeed, the primary function of melanin is to protect the human body from harmful UV radiation [40–42].

##### 3. Dermis

The absorption coefficient of the dermis is determined primarily by the absorption of blood [26,39,46] and can be written as [48,77]

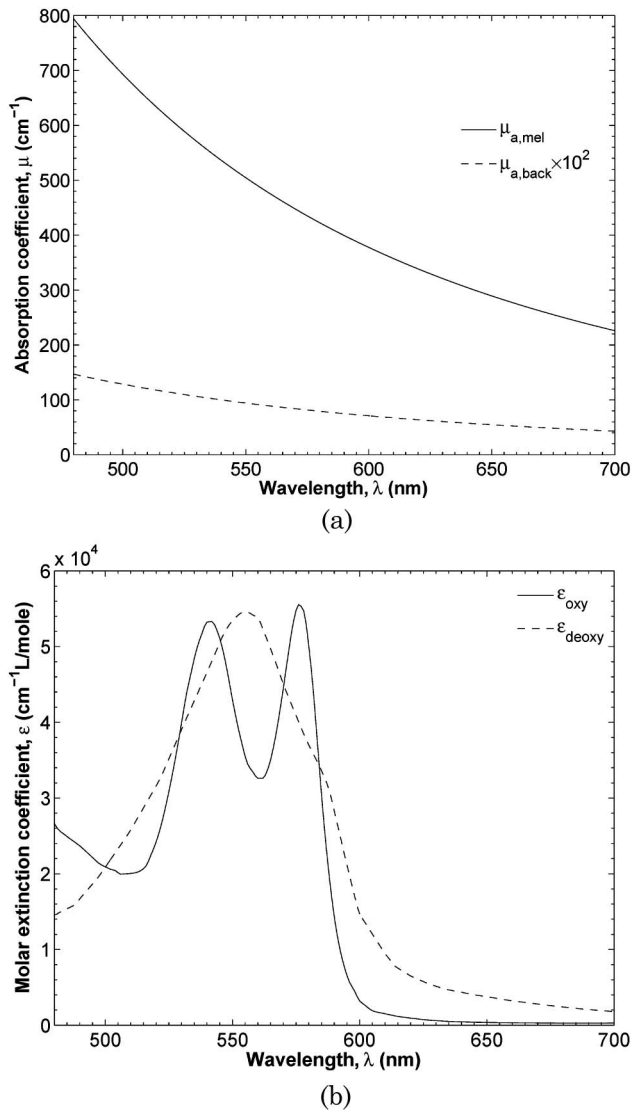


Fig. 2. Absorption properties of endogenous skin chromophores in the visible range (480 to 700 nm). (a) Absorption coefficient of melanosomes [76]. (b) Spectral molar extinction coefficient of human oxyhemoglobin and deoxyhemoglobin [77].

$$\mu_{a,\text{derm}}(\lambda) = f_{\text{blood}}\mu_{a,\text{blood}}(\lambda) + \mu_{a,\text{back}}(\lambda)(1 - f_{\text{blood}}), \quad (14)$$

where  $f_{\text{blood}}$  is the volume fraction of the dermis occupied by blood and  $\mu_{a,\text{back}}(\lambda)$  is given by Eq. (12). In the visible range, oxyhemoglobin and deoxyhemoglobin are mainly responsible for blood absorption, i.e.,  $\mu_{a,\text{blood}}(\lambda) = \mu_{a,\text{oxy}}(\lambda) + \mu_{a,\text{deoxy}}(\lambda)$ . The absorption coefficient of oxyhemoglobin is given by [48,77]

$$\mu_{a,\text{oxy}}(\lambda) = \epsilon_{\text{oxy}}(\lambda)C_{\text{heme}}\text{SO}_2/66,500, \quad (15)$$

where  $\epsilon_{\text{oxy}}(\lambda)$  is the molar extinction coefficient of oxyhemoglobin in  $\text{cm}^{-1}/(\text{mole}/\text{liter})$  of molecular weight 66,500 g/mol while  $C_{\text{heme}}$  is the concentration ratio of hemoglobin in blood (grams/liter), and  $\text{SO}_2$  is the oxygen saturation. Similarly, the absorption coefficient of deoxyhemoglobin is given by [48,77]

$$\mu_{a,\text{deoxy}}(\lambda) = \epsilon_{\text{deoxy}}(\lambda)C_{\text{heme}}(1 - \text{SO}_2)/66,500, \quad (16)$$

where  $\epsilon_{\text{deoxy}}(\lambda)$  is the molar extinction coefficient of deoxyhemoglobin. While the blood volume fraction  $f_{\text{blood}}$  and oxygen saturation  $\text{SO}_2$  may vary with location and metabolic state, the average value of hemoglobin concentration  $C_{\text{heme}}$  is typically constant and equal to 150 g/l [44,77,78]. The spectral molar extinction coefficients of oxyhemoglobin and deoxyhemoglobin are available in the literature for a wide range of wavelengths [77,79–81]. Figure 2(b) shows the values of  $\epsilon_{\text{oxy}}(\lambda)$  and  $\epsilon_{\text{deoxy}}(\lambda)$  used in this study in the visible range from 450 to 700 nm, as reported in the literature [77]. Oxyhemoglobin exhibits two absorption peaks, at 542 and 578 nm, while deoxyhemoglobin exhibits a single peak, at 554 nm. Furthermore, oxyhemoglobin is nearly transparent for wavelengths above 600 nm, giving oxygen rich blood its red color.

### C. Simulated Diffuse Reflectance

The biological properties required to estimate the radiative properties of skin in order to solve the RTE can be represented by the input property vector:

$$\vec{a}_i = \langle f_{\text{mel}}, L_{\text{epi}}, f_{\text{blood}}, \text{SO}_2, C, b \rangle. \quad (17)$$

For a given vector  $\vec{a}_i$ , the absorption and scattering coefficients of the epidermis and dermis were determined as a function of wavelength using Eqs. (10)–(16). Then, the RTE was solved on a spectral basis for 40 evenly spaced wavelengths between 480 and 650 nm using the Monte Carlo simulation software developed by Wang and Jacques [32]. A complete and detailed description of the implementation and theoretical underpinnings of this software is given in Ref. [32]. The number of simulated photon packets per simulation was adjusted until the variance associated with the estimate of the diffuse reflectance fell below 1%. Each Monte Carlo simulation was allowed to run with 1,000,000 photon bundles, which effectively reduced the variance of the simulated diffuse reflectance spectra to zero. The computed diffuse reflectance is referred to as the “simulated diffuse reflectance spectrum,” denoted by  $R_i(\vec{a}_i, \lambda_j)$ , where  $\lambda_j$  is the  $j$ th wavelength and  $j$  is an integer between 1 and  $K$ .

### D. Inverse Method

The goal of the inverse problem was to estimate the vector  $\vec{a}_i$  from the simulated diffuse reflectance  $R_i(\vec{a}_i, \lambda_j)$ . This was achieved by finding an estimate vector  $\vec{a}_e$  that minimizes the sum of the squared residuals  $\delta$  expressed as

$$\delta = \sum_{i=1}^K [R_i(\vec{a}_i, \lambda_j) - R_e(\vec{a}_e, \lambda_j)]^2 W_j^2, \quad (18)$$

where  $R_e(\vec{a}_e, \lambda_j)$  is the estimated spectral diffuse reflectance predicted by Eqs. (4) and (5),  $W_j$  is the

weight associated with the  $j$ th residual, and  $K$  is the number of wavelengths considered. The input diffuse reflectance spectra  $R_i(\vec{a}_i, \lambda_j)$  were calculated by Monte Carlo simulations for a given input parameter vector  $\vec{a}_i$ . Diffuse reflectance was predicted at  $K = 40$  evenly spaced wavelengths between 490 and 650 nm. This wavelength range was chosen such that melanin, oxyhemoglobin, and deoxyhemoglobin exhibit distinct and significant absorption [Figs. 2(a) and 2(b)].

Note that the number of wavelengths considered ( $K = 40$ ) was chosen arbitrarily. Theoretically, six wavelengths are required to retrieve the six unknowns  $f_{mel}$ ,  $L_{epi}$ ,  $f_{blood}$ ,  $SO_2$ ,  $C$ , and  $b$ . In practice, more measurements can be made to reduce the effects of experimental uncertainty. Furthermore, wavelengths can be strategically chosen to coincide with the absorption peaks of oxyhemoglobin and deoxyhemoglobin to increase the inverse method's sensitivity to, for example,  $SO_2$  [13]. The goal of this study, however, was to assess the use of the semiempirical model [Eq. (4)] in predicting  $\vec{a}_i$ . Therefore,  $K$  was chosen to be relatively large, yet practically implementable so as to reduce the effects of numerical error and wavelength selection.

The values of  $W_j$  were chosen to be 2.0 for  $\lambda_j < 600$  nm and 1.0 for  $\lambda_j \geq 600$  nm to increase the method's sensitivity to changes in  $SO_2$  observed mainly for  $\lambda < 600$  nm. Equation (18) was solved iteratively with the constrained Levenberg–Marquardt algorithm [82]. The values of the estimated property vector  $\vec{a}_e$  were constrained between physiologically realistic upper and lower bounds reported in the literature and summarized in Table 1. The minimization was stopped once successive iterations of the algorithm no longer reduced  $\delta$  by more than  $10^{-9}$ . Furthermore, multiple random initial guesses for  $\vec{a}_e$  were attempted to prevent convergence to a local minimum.

#### 4. Results and Discussion

##### A. Accuracy of Semiempirical Model for Skin

Figure 3 compares the diffuse reflectance spectrum  $R_i(\lambda)$  calculated by Monte Carlo simulations to that predicted by Eq. (4) for  $L_{epi} = 30 \mu\text{m}$  and  $f_{mel} = 5.0\%$ . Two different values for both  $f_{blood}$  and  $SO_2$  were explored, namely,  $f_{blood} = 0.41\%$  and  $7\%$  and  $SO_2 = 0\%$  and  $100\%$ . The effects of oxygen saturation on the shape of the diffuse reflectance spectrum was most apparent when  $f_{blood} = 7.0\%$ . Skin with oxygen de-

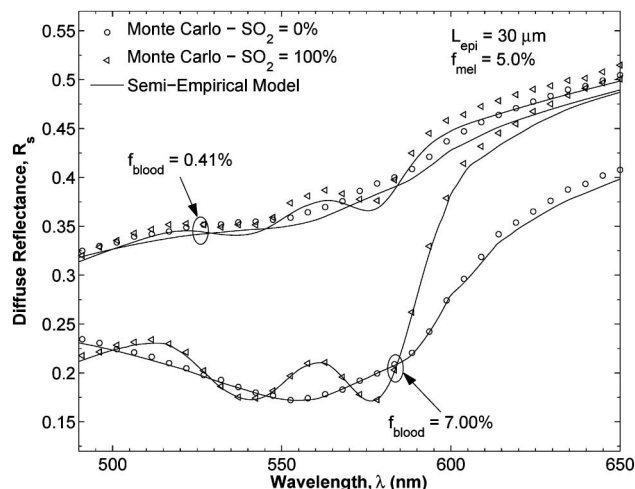


Fig. 3. Diffuse reflectance of human skin as a function of wavelength calculated by Monte Carlo simulations and predicted by the semiempirical model for  $L_{epi} = 30 \mu\text{m}$  and  $f_{mel} = 5.0\%$  and different values of blood volume fraction  $f_{blood}$  (0.41% and 7%) and oxygen saturation  $SO_2$  (0 and 100%).

pleted blood, corresponding to  $SO_2 = 0\%$ , exhibited the single absorption peak of deoxyhemoglobin at 554 nm, while reflectance for  $SO_2 = 100\%$  exhibited both oxyhemoglobin absorption peaks at 542 and 578 nm. Furthermore, fully oxygenated blood resulted in 1.5 times more reflective skin for  $\lambda > 600$  nm than when blood was deoxygenated. Figure 3 also shows that decreasing the blood volume fraction to  $f_{blood} = 0.41\%$  greatly diminished the effects of oxygen saturation on the reflectance spectrum. Then, the oxyhemoglobin and deoxyhemoglobin peaks and changes in reflectance were far more subtle since the absorption coefficient of the dermis predicted by Eq. (14) was dominated by  $\mu_{a,back}$ . Note that it typically took 2 min on a 2.66 GHz processor to compute the diffuse reflectance spectrum for 40 discrete wavelengths using Monte Carlo simulations [32]. On the other hand, the diffuse reflectance spectrum could be estimated nearly instantaneously by using Eqs. (4)–(9).

The accuracy of the semiempirical model with respect to predictions by Monte Carlo simulations can also be assessed from Fig. 3. For  $f_{blood} = 7.0\%$ , predictions of the diffuse reflectance by the semiempirical model fell within 3% of that calculated by Monte Carlo simulations for all wavelengths considered. The error was less than 0.5% for  $\lambda$  between 530 and 600 nm, the region associated with the oxyhemoglobin and

Table 1. Lower and Upper Bound Values for Biological Properties of Human Skin Estimated by the Inverse Method

Biological Property	Symbol	Lower Bound	Upper Bound	Reference
Volume fraction of melanosomes	$f_{mel}$	1%	10%	[40–42]
Epidermal thickness	$L_{epi}$	20 $\mu\text{m}$	150 $\mu\text{m}$	[26,42–44]
Blood volume fraction	$f_{blood}$	0.2%	7%	[42,49]
Oxygen saturation	$SO_2$	0%	100%	
Scattering constant	$C$	$4.0 \times 10^5 \text{ cm}^{-1}$	$5.5 \times 10^5 \text{ cm}^{-1}$	[42]
Scattering power constant	$b$	1.10	1.50	[16,17,42]

deoxyhemoglobin peaks. However, for  $f_{\text{blood}} = 0.41\%$ , the semiempirical model underpredicted the diffuse reflectance by approximately 4% for all wavelengths and for  $\text{SO}_2$  equal to 0% and 100%. As discussed by Yudovsky and Pilon [35], the prediction error associated with the semiempirical model used in this study increased when the transport single scattering albedo of either layer approached unity. Thus, as  $f_{\text{blood}}$  decreased, the absorption coefficient of the dermis  $\mu_{a,\text{derm}}$  decreased and its single scattering albedo approached 1.0, resulting in larger error in the prediction of the diffuse reflectance.

## B. Parameter Estimation

Diffuse reflectance spectra were calculated with Monte Carlo simulations while varying the components of  $\vec{a}_i$  between the upper and lower bounds reported in Table 1. Six values of oxygen saturation  $\text{SO}_2$ , epidermal thickness  $L_{\text{epi}}$ , melanosome volume fraction  $f_{\text{mel}}$ , and blood volume fraction  $f_{\text{blood}}$ , and three values of scattering constants  $C$  and  $b$ , were considered for a total of 11,664 simulated spectra. For each spectrum, the estimate vector  $\vec{a}_e$  was found by minimizing  $\delta$  defined in Eq. (17). To explore the effects of each parameter separately, two scenarios were considered. First, the inverse method's ability to estimate  $L_{\text{epi}}$ ,  $f_{\text{mel}}$ ,  $f_{\text{blood}}$ , and  $\text{SO}_2$  was assessed, assuming that the scattering constants  $C$  and  $b$  were known. Second, the scattering constants  $C$  and  $b$  were assumed unknown and were retrieved along with the other four input parameters. To assess the accuracy of the inverse method, the root-mean-squared (rms) error in the retrieval of a given parameter was computed over the entire range of biological properties considered for an arbitrary value of that parameter.

### 1. Estimation with Known $C$ and $b$

In this section,  $C$  and  $b$  were assumed to be known and equal to  $C = 5.0 \times 10^5 \text{ cm}^{-1}$  and  $b = 1.30$ . These values were measured *ex vivo* for healthy human skin [42]. Here, diffuse reflectance spectra were simulated only for input melanin concentration  $f_{\text{mel}} = 5\%$ . Then, values of  $f_{\text{mel}}$ ,  $L_{\text{epi}}$ ,  $\text{SO}_2$ , and  $f_{\text{blood}}$  were retrieved by the inverse method by using the simulated diffuse reflectance spectrum obtained by using Monte Carlo simulations for the range of  $f_{\text{mel}}$ ,  $L_{\text{epi}}$ ,  $\text{SO}_2$ , and  $f_{\text{blood}}$  specified in Table 1. The rms relative error between the estimated and input value of  $f_{\text{mel}} = 5\%$  was less than 0.5% for all values of  $L_{\text{epi}}$ ,  $\text{SO}_2$ , and  $f_{\text{blood}}$  considered.

Figs. 4(a) and 4(b) show the estimated versus input oxygen saturation  $\text{SO}_2$  and 10% absolute error bounds for  $L_{\text{epi}}$  ranging from 20 to  $150 \mu\text{m}$  and for  $f_{\text{blood}}$  equal to 0.20% and 7.0%, respectively. Figure 4(a) indicates that  $\text{SO}_2$  was overestimated for low values of  $f_{\text{blood}}$ . This was primarily due to the underprediction of diffuse reflectance by the semiempirical model for  $\lambda \geq 600 \text{ nm}$  (Fig. 3). Indeed, highly oxygenated blood exhibited stronger reflectance in this spectral range. Thus, an overestimate of  $\text{SO}_2$  com-

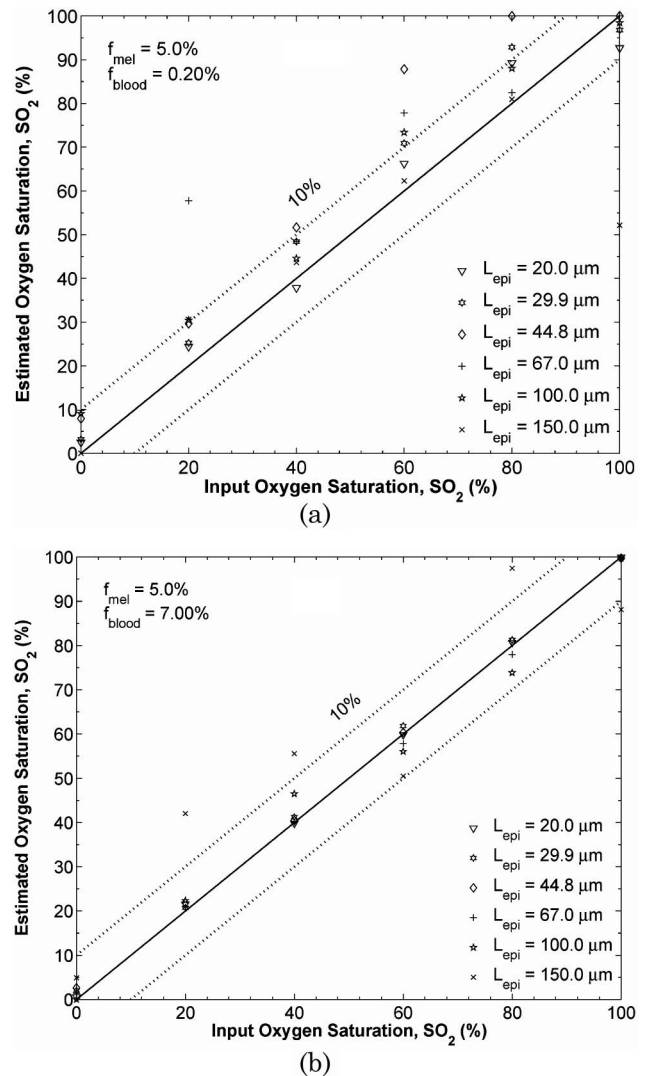


Fig. 4. Estimated versus input oxygen saturation  $\text{SO}_2$  and 10% absolute error bounds for input values  $f_{\text{mel}} = 5.0\%$ ,  $20 \leq L_{\text{epi}} \leq 150 \mu\text{m}$ , and (a)  $f_{\text{blood}} = 0.20\%$  and (b) 7%, respectively. The scattering constants were taken as  $C = 5.0 \times 10^5 \text{ cm}^{-1}$  and  $b = 1.30$ .

pensated for the inaccuracy of the semiempirical model. Figure 4(a) also shows the effect of epidermal thickness on the prediction of  $\text{SO}_2$ . A thicker epidermis resulted in poorer estimates of  $\text{SO}_2$  because, then, the epidermis optically shielded the dermis. The effect of epidermal thickness on the prediction of  $\text{SO}_2$  was best illustrated for input  $\text{SO}_2 = 60\%$ . In this case, when  $L_{\text{epi}} = 20 \mu\text{m}$ , the absolute estimation error was less than 5%. However, for  $L_{\text{epi}}$  larger than  $100 \mu\text{m}$ , the absolute error in  $\text{SO}_2$  increased beyond 10%.

Figure 4(b) indicates that, for blood volume equal to 7.0%, epidermal thickness has little effect on the prediction error associated with  $\text{SO}_2$ . The rms and the maximum absolute errors between the estimated and input values of  $\text{SO}_2$  increased from 2.9% and 9.2% to 13.5% and 47.9%, respectively, as  $L_{\text{epi}}$  increased from 20 to  $150 \mu\text{m}$ . In contrast, as  $f_{\text{blood}}$  increased from 0.20% to 7.0%, the rms and maximum

absolute errors between the estimated and input values of  $SO_2$  decreased from 13.8% to 3% and from 47.9% to 9.4%, respectively. The largest maximum error of 47.9% occurred for the lowest values of  $f_{\text{blood}}$  and the largest values of  $L_{\text{epi}}$ . However, it was not typical of this inverse method's performance, as suggested by the rms error. Nouvong *et al.* [54] recently measured the oxygen saturation near healing and nonhealing diabetic foot ulcers using hyperspectral imaging [12]. Their data suggests that skin near nonhealing ulcers exhibit a 10% lower oxygen saturation on average when compared with skin near healing ulcers. Furthermore, the values of  $SO_2$  reported were near 55%. The rms error of the present algorithm for  $SO_2 = 55\%$  was found to be 3.6%. Thus, the present method is accurate enough to assess wound healing on the diabetic foot.

Figures 5(a) and 5(b) show the estimated versus input values of  $f_{\text{blood}}$  and 0.5% absolute error bounds for  $20 \leq L_{\text{epi}} \leq 150 \mu\text{m}$  and  $SO_2 = 0\%$  and 100%, respectively. Unlike the estimate of  $SO_2$  previously discussed, the estimate of  $f_{\text{blood}}$  was almost unaffected by epidermal thickness  $L_{\text{epi}}$  because the effect of increasing or decreasing  $f_{\text{blood}}$  was to shift the entire reflectance spectrum intensity down or up, respectively. Changes in  $SO_2$ , on the other hand, affected the spectral shape of the diffuse reflectance spectrum near the absorption peaks of oxyhemoglobin and deoxyhemoglobin ( $530 < \lambda < 600 \text{ nm}$ ). However,  $SO_2$  had an effect only outside of this wavelength range for larger values of  $f_{\text{blood}}$ . Thus, the proposed inverse method predicted changes in  $f_{\text{blood}}$  more accurately than changes in  $SO_2$ . Furthermore, as  $L_{\text{epi}}$  increased from 20 to  $150 \mu\text{m}$ , the rms and the maximum absolute errors between the input and estimated values of  $f_{\text{blood}}$  increased from 0.074% to 0.21% and from 0.30% to 0.71%, respectively. However, these errors remained small and acceptable for all values of  $L_{\text{epi}}$ .

Figures 6(a) and 6(b) show the estimated versus input values of  $L_{\text{epi}}$  and 10% relative error bounds for  $SO_2$  between 0% and 100% and for  $f_{\text{blood}} = 0.20\%$  and 7.0%, respectively. The relative error in  $L_{\text{epi}}$  was larger than 10% for  $f_{\text{blood}}$  less than 1% and  $L_{\text{epi}}$  between 40 and  $100 \mu\text{m}$ . However, for  $L_{\text{epi}}$  smaller than  $40 \mu\text{m}$  or larger than  $100 \mu\text{m}$ , the epidermal thickness was dominant in determining the shape of the diffuse reflectance spectrum. In both cases,  $L_{\text{epi}}$  was estimated accurately for all values of  $f_{\text{blood}}$ . Indeed, for large values of  $f_{\text{blood}}$ ,  $\omega_{\text{tr,derm}}$  decreased but remained larger than 0.5, resulting in better agreement between the semiempirical model and the Monte Carlo simulations. Thus, the epidermal thickness  $L_{\text{epi}}$  was better estimated for larger values of  $f_{\text{blood}}$ . In fact, as  $f_{\text{blood}}$  increased from 0.20% to 7.0%, the rms relative error and the maximum relative error between the input and estimated values of  $L_{\text{epi}}$  decreased from 8.1% to 6.6% and from 20.1% to 16.7%, respectively. Note that, for all cases, the maximum absolute error in estimating  $L_{\text{epi}}$  was less than

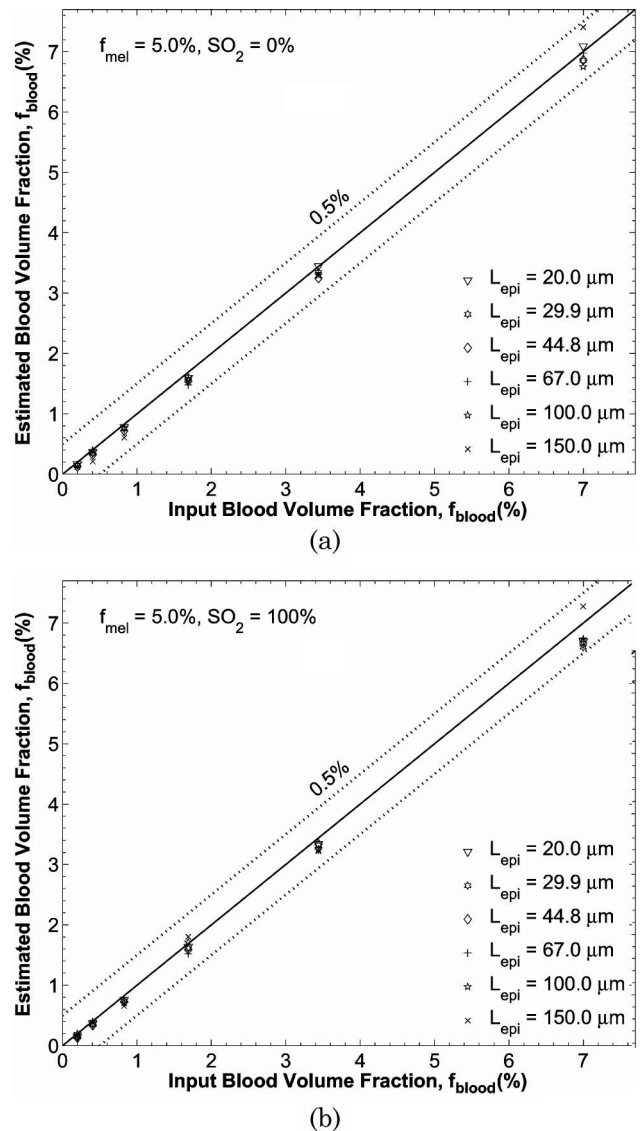
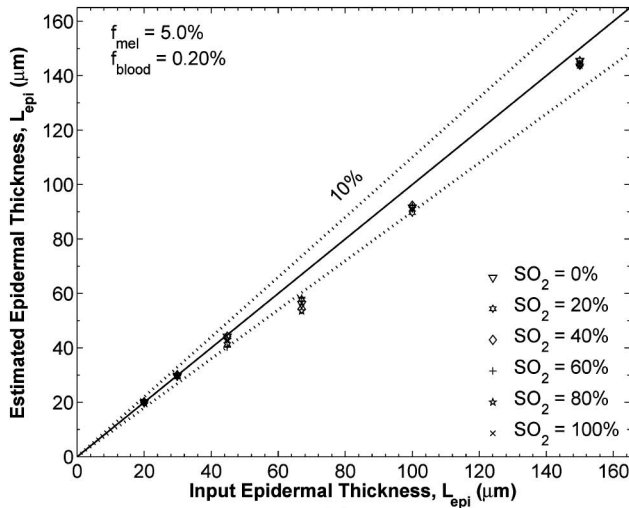


Fig. 5. Estimated versus input blood volume fraction  $f_{\text{blood}}$  and 0.5% absolute error bounds for input values  $f_{\text{mel}} = 5.0\%$ ,  $20 \leq L_{\text{epi}} \leq 150 \mu\text{m}$ , and (a)  $SO_2 = 0\%$  and (b)  $100\%$ , respectively. The scattering constants were taken as  $C = 5.0 \times 10^5 \text{ cm}^{-1}$  and  $b = 1.30$ .

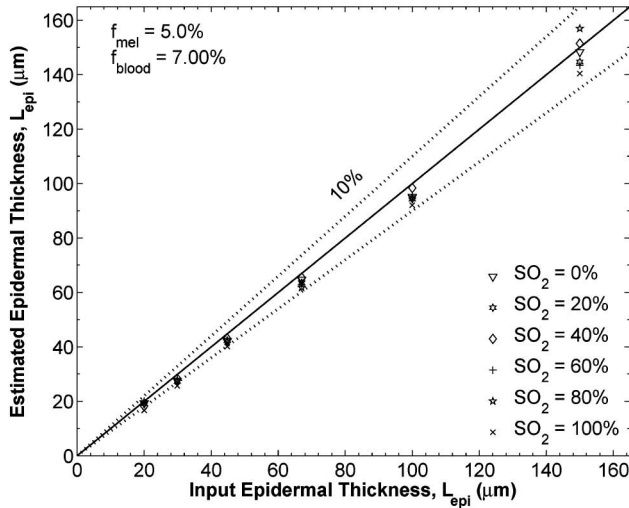
$14 \mu\text{m}$ , which is approximately the diameter of a keratinocyte cell [83].

## 2. Estimation of Melanin Concentration

Here also,  $C$  and  $b$  were assumed to be known and equal to  $C = 5.0 \times 10^5 \text{ cm}^{-1}$  and  $b = 1.30$ . The value of  $f_{\text{mel}}$  was varied between 1% and 10% and was retrieved by the inverse method along with  $L_{\text{epi}}$ ,  $SO_2$ , and  $f_{\text{blood}}$ . While melanosome volume fractions of up to 43% have been reported [42], the range considered in this study was abridged to 10%. Indeed, beyond 10%, the transport single scattering albedo  $\omega_{\text{tr,epi}}$  became less than 0.50 and the accuracy of the semiempirical model in predicting the diffuse reflectance greatly diminished [35], making accurate inversion difficult or even impossible.



(a)



(b)

Fig. 6. Estimated versus input epidermal thickness  $L_{\text{epi}}$  and 10% relative error bounds for input values  $f_{\text{mel}} = 5.0\%$ ,  $0\% \leq \text{SO}_2 \leq 100\%$ , and (a)  $f_{\text{blood}} = 0.20\%$  and (b)  $7.0\%$ , respectively. The scattering constants were taken as  $C = 5.0 \times 10^5 \text{ cm}^{-1}$  and  $b = 1.30$ .

Figure 7 shows the estimated versus input values of  $f_{\text{mel}}$  and 0.5% absolute error bounds for various input values of  $L_{\text{epi}}$  and  $f_{\text{blood}}$ , and for  $\text{SO}_2 = 50\%$ . The estimate of  $f_{\text{mel}}$  was well within 0.5% for all values of  $L_{\text{epi}}$ . As with  $f_{\text{blood}}$ , shown in Fig. 5, the absolute error was small and acceptable. Similar results as those discussed in Subsection 4.B.1 for  $f_{\text{mel}} = 5\%$  were found for the retrieved values of  $\text{SO}_2$ ,  $L_{\text{epi}}$ , and  $f_{\text{blood}}$  and need not be repeated. In other words, the ability of the inverse method to estimate  $L_{\text{epi}}$ ,  $\text{SO}_2$ , and  $f_{\text{blood}}$  was not altered by the melanosome volume fraction  $f_{\text{mel}}$ .

### 3. Estimation of Tissue Scattering

So far, the values of  $C$  and  $b$  were considered to be constant and known. In reality, they depend on the average diameter and concentration of collagen fibers in the skin, for example. They may vary from

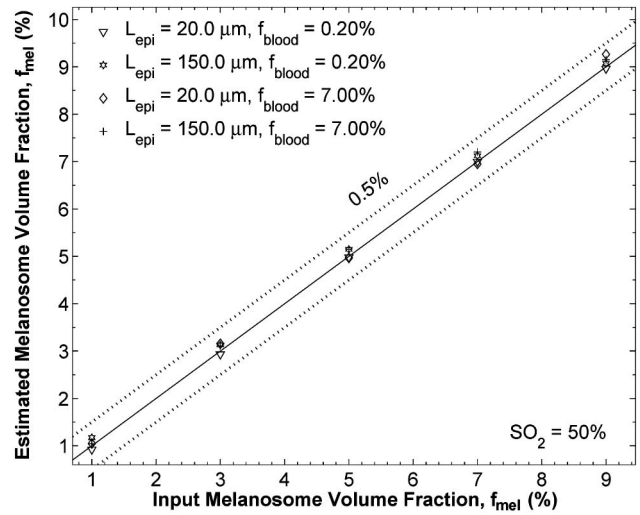


Fig. 7. Estimated versus input melanosome volume fraction  $f_{\text{mel}}$  and 0.5% absolute error bounds for input values  $20 \leq L_{\text{epi}} \leq 150 \mu\text{m}$  and  $0.20 \leq f_{\text{blood}} \leq 7.0\%$ , and  $\text{SO}_2 = 50\%$ . The scattering constants were taken as  $C = 5.0 \times 10^5 \text{ cm}^{-1}$  and  $b = 1.30$ .

$4.0 \times 10^5$  to  $5.5 \times 10^5 \text{ cm}^{-1}$  and from 1.1 to 1.5, respectively [17,18,70]. To test the ability of the proposed inverse method to estimate  $C$  and  $b$  from diffuse reflectance measurements, Monte Carlo simulations were performed while varying  $C$  and  $b$  between these bounds. Then,  $\delta$  given by Eq. (18) was minimized to find optimal estimates of  $C$  and  $b$  for each diffuse reflectance spectrum, in addition to the four parameters  $f_{\text{mel}}$ ,  $L_{\text{epi}}$ ,  $f_{\text{blood}}$ , and  $\text{SO}_2$ . It was found that  $f_{\text{mel}}$ ,  $L_{\text{epi}}$ ,  $f_{\text{blood}}$ ,  $\text{SO}_2$ , and  $b$  or  $C$  could be estimated accurately only if  $C$  or  $b$  was assumed to be known, respectively. However, if both  $b$  and  $C$  were retrieved simultaneously, only  $\text{SO}_2$ ,  $f_{\text{mel}}$ , and  $L_{\text{epi}}$  could be estimated reliably, while  $f_{\text{blood}}$ ,  $b$ , and  $C$  could not be accurately estimated. This was despite the fact that the estimated diffuse reflectance by the semiempirical model using the retrieved parameters matched the input diffuse reflectance closely for all cases considered.

Therefore, values of  $b$  measured *in vitro* and reported in the literature [16,17,42] were used in conjunction with the present inverse method. Figures 8(a) and 8(b) show the estimated versus input scattering constant  $C$  and 5% relative error bounds for  $20 \leq L_{\text{epi}} \leq 150 \mu\text{m}$ ,  $0.20\% \leq f_{\text{blood}} \leq 7\%$ ,  $f_{\text{mel}} = 5\%$ , and for  $\text{SO}_2 = 0\%$  and  $100\%$ , respectively. The parameter  $b$  was assumed to be constant and equal to 1.30 for both simulated and estimated diffuse reflectance. The blood volume fraction  $f_{\text{blood}}$  had the strongest effect on the relative error in the retrieved  $C$ . Greater error was observed for small values of  $f_{\text{blood}}$  for reasons previously discussed (Subsection 4.B.1). As  $f_{\text{blood}}$  increased from 0.20% to 7.0%, the rms relative error and the maximum relative error between the input and estimated values of  $C$  decreased from 5.9% to 1.4% and from 23.4% to 3.4%, respectively. These errors remained small and acceptable.

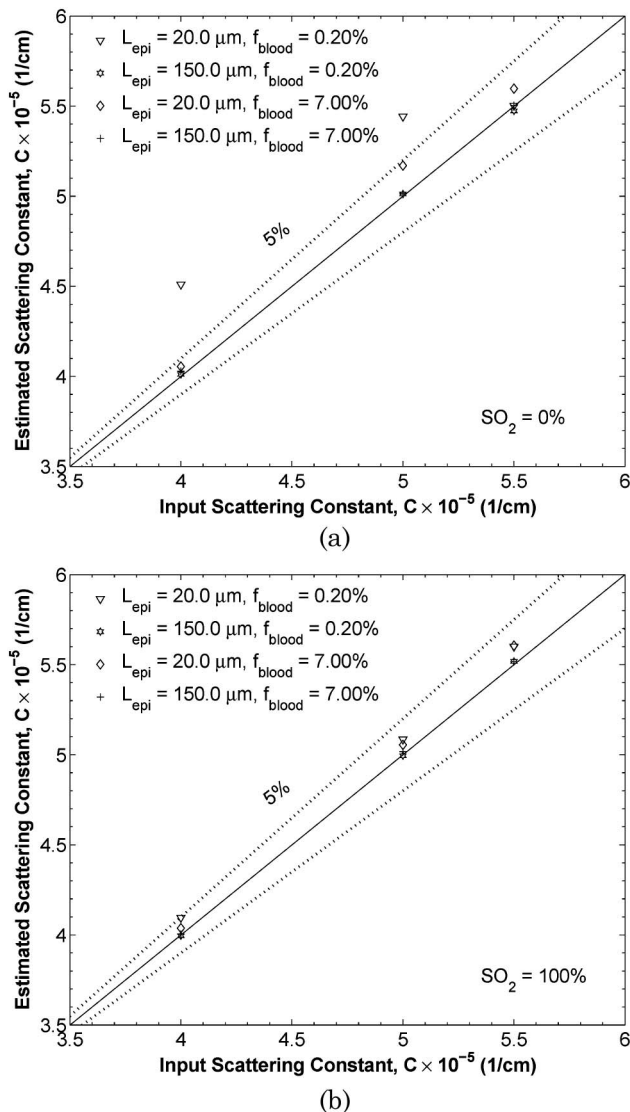


Fig. 8. Estimated versus input scattering constant  $C$  and 5% relative error bounds for input values  $20 \leq L_{\text{epi}} \leq 150 \mu\text{m}$ ,  $0.20 \leq f_{\text{blood}} \leq 7.0\%$ ,  $f_{\text{mel}} = 5.0\%$ , and  $b = 1.30$  for (a)  $\text{SO}_2 = 0\%$  and (b)  $\text{SO}_2 = 100\%$ . The scattering constant  $b$  is assumed to be known.

To illustrate the accuracy of the inverse method using the semiempirical model, simulated diffuse reflectance spectra were produced for  $L_{\text{epi}} = 50$  and  $100 \mu\text{m}$  and  $f_{\text{mel}}$  equal to 1%, 5%, and 10%, representing weakly, moderately, and strongly pigmented skin, respectively. The input values of the other param-

eters  $\text{SO}_2$ ,  $f_{\text{blood}}$ , and  $C$  were chosen in the ranges given in Table 1. Then, all five parameters were estimated, while  $b$  was imposed to be 1.30. Table 2 shows the relative rms error between the input and estimated values of  $f_{\text{mel}}$ ,  $L_{\text{epi}}$ ,  $f_{\text{blood}}$ ,  $\text{SO}_2$ , and  $C$  for the three skin complexions and two epidermal thicknesses considered. Note that input values of  $\text{SO}_2$  smaller than 25% were ignored while calculating the relative rms error associated with estimating  $\text{SO}_2$  because these small values are unrealistic for living tissues.

Finally, the present inverse algorithm was recently used to detect callus and ulcer formation on the foot of a diabetic patient [84]. Hyperspectral tissue reflectance images of the foot of a diabetic patient were collected at regular interval for 18 months [54]. During this period, a foot ulcer developed on the plantar surface of the left sole [54]. Hyperspectral data of the ulceration site was available 30 days before the ulcer formed. A diabetic foot ulcer is often preceded by callus formation (i.e., epidermal thickening) around the preulcerative site [85,86]. As the ulcer formation progresses, the epidermis immediately above the necrotic tissue diminishes in thickness [85,86]. Estimation of the epidermal thickness was performed with the present algorithm to confirm that such changes could be detected optically. In fact, the preulcerative site exhibited an epidermal thickness of  $85 \mu\text{m}$  and was surrounded by much thicker epidermis of approximately  $130 \mu\text{m}$ . These results show promise that the present algorithm could be used to assess tissue health *in vivo* and in a clinical setting. However, complete discussion of this topic falls outside the scope of this paper.

## 5. Conclusion

In this paper, human skin was modeled as a slab of variable thickness, corresponding to the epidermis, supported by a semi-infinite layer, corresponding to the dermis. Absorption in the epidermis was due to melanin and varied depending on the melanosome volume fraction. Absorption in the epidermis was due to oxyhemoglobin and deoxyhemoglobin and varied with blood volume fraction and oxygen saturation. The index of refraction and the scattering coefficient in both layers were assumed to be identical. The radiative transfer equation was solved on a spectral basis between 490 and 650 nm by Monte Carlo simulations, to produce simulated diffuse

Table 2. Relative RMS Error between Retrieved and Input Values of  $f_{\text{mel}}$ ,  $L_{\text{epi}}$ ,  $\text{SO}_2$ ,  $f_{\text{blood}}$ , and  $C$  for  $L_{\text{epi}} = 50$  and  $100 \mu\text{m}$  and  $f_{\text{mel}}$  Equal to 1%, 5%, and 10%, Representing Weakly, Moderately, and Strongly Pigmented Skin, Respectively<sup>a</sup>

$f_{\text{mel}}$	$L_{\text{epi}} = 50 \mu\text{m}$					$L_{\text{epi}} = 100 \mu\text{m}$				
	$f_{\text{mel}}$	$L_{\text{epi}}$	$\text{SO}_2$	$f_{\text{blood}}$	$C$	$f_{\text{mel}}$	$L_{\text{epi}}$	$\text{SO}_2$	$f_{\text{blood}}$	$C$
1%	9.3%	16.1%	1.3%	2.5%	2.4%	10.1%	15.4%	4.8%	5.2%	2.2%
5%	9.9%	9.6%	4.6%	10.2%	2.4%	3.7%	5.7%	4.9%	6.4%	2.5%
10%	3.5%	1.8%	3.2%	11.8%	3.1%	0.5%	3.8%	15.8%	11.3%	2.2%

<sup>a</sup>The input values of  $\text{SO}_2$ ,  $f_{\text{blood}}$ , and  $C$  were chosen in the ranges given in Table 1. The rms error in estimating  $\text{SO}_2$  was calculated for  $\text{SO}_2 > 25\%$ .

reflectance spectra for a wide range of biological properties. Then, an inverse method was used to retrieve physiologically meaningful parameters from the simulated diffuse reflectance spectra. A quicker semiempirical model [35] was used instead of Monte Carlo simulations in the iterative inversion procedure. The accuracy of the inverse method in estimating  $f_{\text{mel}}$ ,  $L_{\text{epi}}$ ,  $\text{SO}_2$ ,  $f_{\text{blood}}$ , and  $C$  was explored for a range of physiologically meaningful values specified in Table 1. In summary, all parameters could be estimated with relative rms error of less than 5% for  $f_{\text{mel}}$  between 1% and 8%,  $L_{\text{epi}}$  ranging from 20 to 150  $\mu\text{m}$ ,  $\text{SO}_2$  from 25% to 100%,  $f_{\text{blood}}$  from 1.2% to 10%, and  $C$  from  $4.0 \times 10^5$  to  $5.5 \times 10^5 \text{ cm}^{-1}$ . The methodology presented can be applied to any two-layer optical system where scattering dominates over absorption.

This research was funded in part through a grant from the National Institute of Diabetes and Digestive and Kidney Diseases (R42-DK069871) through HyperMed, Inc. The authors would like to thank A. Nouvong, K. Schomacker, and R. Lifshitz for useful discussion and exchange of information.

## References

- G. Zonios, A. Dimou, I. Bassukas, D. Galaris, A. Tsolakidis, and E. Kaxiras, "Melanin absorption spectroscopy: new method for noninvasive skin investigation and melanoma detection," *J. Biomed. Opt.* **13**, 014017 (2008).
- W. M. Kuebler, "How NIR is the future in blood flow monitoring?," *J. Appl. Physiol.* **104**, 905–906 (2008).
- R. L. P. van Veen, A. Amelink, M. Menke-Pluymers, C. van der Pol, and H. Sterenberg, "Optical biopsy of breast tissue using differential path-length spectroscopy," *Phys. Med. Biol.* **50**, 2573–2581 (2005).
- L. Khaodhiar, T. Dinh, K. T. Schomacker, S. V. Panasyuk, J. E. Freeman, R. Lew, T. Vo, A. A. Panasyuk, C. Lima, J. M. Giurini, T. E. Lyons, and A. Veves, "The use of medical hyperspectral technology to evaluate microcirculatory changes in diabetic foot ulcers and to predict clinical outcomes," *Diabetes Care* **30**, 903–910 (2007).
- A. Torricelli, D. Contini, A. Pifferi, L. Spinelli, and R. Cubeddu, "Functional brain imaging by multi-wavelength time-resolved near infrared spectroscopy," *Opto-Electron. Rev.* **16**, 131–135 (2008).
- N. Tsumura, M. Kawabuchi, H. Haneishi, and Y. Miyake, "Mapping pigmentation in human skin from multi-visible spectral imaging by inverse optical scattering technique," in *Proceedings of the Eighth Color Imaging Conference: Color Science, Systems and Applications* (Society for Imaging Science and Technology, 2000), pp. 444–450.
- N. Tsumura, H. Haneishi, and Y. Miyake, "Independent-component analysis of skin color image," *J. Opt. Soc. Am. A* **16**, 2169–2176 (1999).
- A. Vogel, V. V. Chernomordik, J. D. Riley, M. Hassan, F. Amyot, B. Dasgeb, S. G. Demos, R. Pursley, R. F. Little, R. Yarchoan, T. Tao, and A. H. Gandjbakhche, "Using noninvasive multispectral imaging to quantitatively assess tissue vasculature," *J. Biomed. Opt.* **12**, 051604 (2007).
- N. Tsumura, R. Usuba, K. Takase, T. Nakaguchi, N. Ojima, N. Komeda, and Y. Miyake, "Image-based control of skin translucency," *Appl. Opt.* **47**, 6543–6549 (2008).
- L. Kocsis, P. Herman, and A. Eke, "The modified Beer-Lambert law revisited," *Phys. Med. Biol.* **51**, N91–N98 (2006).
- N. Tsumura, T. Nakaguchi, N. Ojima, K. Takase, S. Okaguchi, K. Hori, and Y. Miyake, "Image-based control of skin melanin texture," *Appl. Opt.* **45**, 6626–6633 (2006).
- K. J. Zuzak, M. D. Schaeberle, E. N. Lewis, and I. W. Levin, "Visible reflectance hyperspectral imaging: characterization of a noninvasive, *in-vivo* system for determining tissue perfusion," *Anal. Chem.* **74**, 2021–2028 (2002).
- S. J. Matcher, C. E. Elwell, C. E. Cooper, M. Cope, and D. T. Delpy, "Performance comparison of several published tissue near-infrared spectroscopy algorithms," *Anal. Biochem.* **227**, 54–68 (1995).
- A. Sassaroli and S. Fantini, "Comment on the modified Beer-Lambert law for scattering media," *Phys. Med. Biol.* **49**, N255–N257 (2004).
- M. F. Modest, *Radiative Heat Transfer* (Academic, 2003).
- R. M. P. Doornbos, R. Lang, M. C. Aalders, F. W. Cross, and H. Sterenberg, "The determination of in vivo human tissue optical properties and absolute chromophore concentrations using spatially resolved steady-state diffuse reflectance spectroscopy," *Phys. Med. Biol.* **44**, 967–982 (1999).
- A. M. K. Nilsson, C. Stureson, D. L. Liu, and S. Andersson-Engels, "Changes in spectral shape of tissue optical properties in conjunction with laser-induced thermotherapy," *Appl. Opt.* **37**, 1256–1267 (1998).
- I. S. Saidi, S. L. Jacques, and F. K. Tittel, "Mie and Rayleigh modeling of visible-light scattering in neonatal skin," *Appl. Opt.* **34**, 7410–7418 (1995).
- J. M. Schmitt and G. Kumar, "Optical scattering properties of soft tissue: a discrete particle model," *Appl. Opt.* **37**, 2788 (1998).
- R. L. P. van Veen, A. Amelink, M. Menke-Pluymers, C. van der Pol, and H. Sterenberg, "Optical biopsy of breast tissue using differential path-length spectroscopy," *Phys. Med. Biol.* **50**, 2573–2581 (2005).
- J. C. Finlay and T. H. Foster, "Hemoglobin oxygen saturations in phantoms and in vivo from measurements of steady-state diffuse reflectance at a single, short source-detector separation," *Med. Phys.* **31**, 1949–1959 (2004).
- E. Okada, M. Firbank, and D. T. Delpy, "The effect of overlying tissue on the spatial sensitivity profile of near-infrared spectroscopy," *Phys. Med. Biol.* **40**, 2093–2108 (1995).
- M. Hiraoka, M. Firbank, M. Essenpreis, M. Cope, S. R. Arridge, P. Zee, and D. T. Delpy, "A Monte Carlo investigation of optical pathlength in inhomogeneous tissue and its application to near-infrared spectroscopy," *Phys. Med. Biol.* **38**, 1859–1876 (1993).
- H. Gray, *Gray's Anatomy* (Bounty, 1977), pp. 1082–1085.
- R. J. Hunter, M. S. Patterson, T. J. Farrell, and J. E. Hayward, "Haemoglobin oxygenation of a two-layer tissue-simulating phantom from time-resolved reflectance: effect of top layer thickness," *Phys. Med. Biol.* **47**, 193–208 (2002).
- R. R. Anderson and J. A. Parrish, "The optics of human skin," *J. Invest. Dermatol.* **77**, 13–19 (1981).
- Y. Lee and K. Hwang, "Skin thickness of Korean adults," *Surg. Radiol. Anat.* **24**, 183–189 (2002).
- M. C. Branchet, S. Boisnic, C. Frances, and A. M. Robert, "Skin thickness changes in normal aging skin," *Gerontology (Basel)* **36**, 28–35 (1990).
- D. E. Barker, "Skin thickness in the human," *Plast. Reconstr. Surg.* **7**, 115–116 (1951).
- K. M. Katika and L. Pilon, "Steady-state directional diffuse reflectance and fluorescence of human skin," *Appl. Opt.* **45**, 4174–4183 (2006).
- H. Zeng, C. E. MacAulay, B. Palcic, and D. I. McLean, "Monte Carlo modeling of tissue autofluorescence measurement and imaging," *Proc. SPIE* **2135**, 94–104 (1994).
- L. Wang and S. L. Jacques, "Monte Carlo modeling of light transport in multi-layered tissues in standard  $C$ ," last

accessed 31 March 2009, <http://labs.seas.wustl.edu/bme/Wang/mcr5/Mcman.pdf>.

33. V. V. Tuchin, *Tissue Optics: Light Scattering Methods and Instruments for Medical Diagnosis* (SPIE, 2007).
34. G. Mantis and G. Zonios, "Simple two-layer reflectance model for biological tissue applications," *Appl. Opt.* **48**, 3490–3496 (2009).
35. D. Yudovsky and L. Pilon, "Simple and accurate expressions for diffuse reflectance of semi-infinite and two-layer absorbing and scattering media," *Appl. Opt.* **48**, 6670–6683 (2009).
36. N. Tsumura, D. Kawazoe, T. Nakaguchi, N. Ojima, and Y. Miyake, "Regression-based model of skin diffuse reflectance for skin color analysis," *Opt. Rev.* **15**, 292–294 (2008).
37. C. M. Gardner, S. L. Jacques, and A. J. Welch, "Light transport in tissue: accurate expressions for one-dimensional fluence rate and escape function based upon Monte Carlo simulation," *Lasers Surg. Med.* **18**, 129–138 (1996).
38. J. Wu, F. Partovi, M. S. Field, and R. P. Rava, "Diffuse reflectance from turbid media: an analytical model of photon migration," *Appl. Opt.* **32**, 1115–1121 (1993).
39. A. R. Young, "Chromophores in human skin," *Phys. Med. Biol.* **42**, 789–802 (1997).
40. T. Dwyer, G. Prota, L. Blizzard, R. Ashbolt, and M. R. Vincensi, "Melanin density and melanin type predict melanocytic naevi in 19–20 year olds of northern European ancestry," *Melanoma research* **10**, 387–394 (2000).
41. T. Dwyer, H. K. Muller, L. Blizzard, R. Ashbolt, and G. Phillips, "The use of spectrophotometry to estimate melanin density in Caucasians," *Cancer Epidemiol. Biomarkers Prev.* **7**, 203–206 (1998).
42. S. L. Jacques, "Origins of tissue optical properties in the UVA, visible, and NIR regions," in *Advances in Optical Imaging and Photon Migration*, R. R. Alfano and J. G. Fujimoto, eds. (Optical Society of America, 1996), Vol. 2, pp. 364–370.
43. M. Doi and S. Tominaga, "Spectral estimation of human skin color using the Kubelka-Munk theory," *Proc. SPIE* **5008**, 221–228 (2003).
44. R. Flewelling, "Noninvasive optical monitoring," in *The Biomedical Engineering Handbook*, J. Bronzoni, ed. (IEEE, 1981), pp. 1–11.
45. I. V. Meglinski and S. J. Matcher, "Modeling of skin reflectance spectra," *Proc. SPIE*, **4241**, 78–87 (2001).
46. M. J. C. Van Gemert, A. J. Welch, W. M. Star, M. Motamedi, and W. F. Cheong, "Tissue optics for a slab geometry in the diffusion approximation," *Lasers Med. Sci.* **2**, 295–302 (1987).
47. W. F. Southwood, "The thickness of the skin," *Plast. Reconstr. Surg.* **15**, 423–429 (1955).
48. A. Krishnaswamy and G. V. G. Baranoski, "A biophysically-based spectral model of light interaction with human skin," in *Computer Graphics Forum* (Blackwell, 2004), Vol. 23, pp. 331–340.
49. E. Angelopoulou, "Understanding the color of human skin," *Proc. SPIE* **4299**, 243–251 (2001).
50. P. Clarys, K. Alewaeters, R. Lambrecht, and A. O. Barel, "Skin color measurements: comparison between three instruments: the Chromameter, the DermaSpectrometer and the Mexameter," *Skin Res. Technol.* **6**, 230–238 (2000).
51. T. Kono, A. R. Erçögen, H. Nakazawa, T. Honda, N. Hayashi, and M. Nozaki, "The flashlamp-pumped pulsed dye laser (585 nm) treatment of hypertrophic scars in Asians," *Ann. Plast. Surg.* **51**, 366–371 (2003).
52. H. J. Yoon, D. H. Lee, S. O. Kim, K. C. Park, and S. W. Youn, "Acne erythema improvement by long-pulsed 595 nm pulsed-dye laser treatment: A pilot study," *J. Derm. Treat.* **19**, 38–44 (2008).
53. R. L. Greenman, S. Panasyuk, X. Wang, T. E. Lyons, T. Dinh, L. Longoria, J. M. Giurini, J. Freeman, L. Khaodhiar, and A. Veves, "Early changes in the skin microcirculation and muscle metabolism of the diabetic foot," *Lancet* **366**, 1711–1717 (2005).
54. A. Nouvong, B. Hoogwerf, E. Mohler, B. Davis, A. Tajaddini, and E. Medenilla, "Evaluation of diabetic foot ulcer healing with hyperspectral imaging of oxyhemoglobin and deoxyhemoglobin," *Diabetes Care* **32**, 2056–2061 (2009).
55. J. Sandby-Moller, T. Poulsen, and H. C. Wulf, "Epidermal thickness at different body sites: relationship to age, gender, pigmentation, blood content, skin type and smoking habits," *Acta Derm. Venereol.* **83**, 410–413 (2003).
56. T. Gambichler, J. Huyn, N. S. Tomi, G. Moussa, C. Moll, A. Sommer, P. Altmeyer, and K. Hoffmann, "A comparative pilot study on ultraviolet-induced skin changes assessed by noninvasive imaging techniques *in vivo*," *Photochem. Photobiol.* **82**, 1103–1107 (2006).
57. J. Lock-Andersen, P. Therkildsen, O. F. de Fine, M. Gniadecka, K. Dahlstrøm, T. Poulsen, and H. C. Wulf, "Epidermal thickness, skin pigmentation and constitutive photosensitivity," *Photodermatol. Photoimmunol. Photomed.* **13**, 153–158 (1997).
58. T. Gambichler, R. Matip, G. Moussa, P. Altmeyer, and K. Hoffmann, "In vivo data of epidermal thickness evaluated by optical coherence tomography: effects of age, gender, skin type, and anatomic site," *J. Dermatol. Sci.* **44**, 145–152 (2006).
59. P. P. Guastalla, V. I. Guerri, A. Fabretto, F. Faletra, D. L. Grasso, E. Zocconi, D. Stefanidou, P. D'Adamo, L. Ronfani, M. Montico, M. Morgutti, and P. Gasparini, "Detection of epidermal thickening in GJB2 carriers with epidermal US," *Radiology* (Oak Brook, Ill.) **251**, 280–286 (2009).
60. D. J. Faber and T. G. van Leeuwen, "Are quantitative attenuation measurements of blood by optical coherence tomography feasible?," *Opt. Lett.* **34**, 1435–1437 (2009).
61. D. J. Faber, E. G. Mik, M. C. G. Aalders, and T. G. van Leeuwen, "Toward assessment of blood oxygen saturation by spectroscopic optical coherence tomography," *Opt. Lett.* **30**, 1015–1017 (2005).
62. L. G. Henyey and J. L. Greenstein, "Diffuse radiation in the galaxy," *Ann. Astrophys.* **93**, 70–83 (1940).
63. M. J. C. Van Gemert, S. L. Jacques, H. Sterenberg, and W. M. Star, "Skin optics," *IEEE Trans. Biomed. Eng.* **36**, 1146–1154 (1989).
64. S. L. Jacques, C. A. Alter, and S. A. Prahl, "Angular dependence of HeNe laser light scattering by human dermis," *Lasers Life Sci.* **1**, 309–334 (1987).
65. S. K. Chang, D. Arifler, R. Drezek, M. Follen, and R. Richards-Kortum, "Analytical model to describe fluorescence spectra of normal and preneoplastic epithelial tissue: comparison with Monte Carlo simulations and clinical measurements," *J. Biomed. Opt.* **9**, 511–522 (2004).
66. I. Lux and L. Koblinger, *Monte Carlo Particle Transport Methods: Neutron and Photon Calculations*, 6th ed. (CRC Press, 1991).
67. M. J. C. van Gemert and W. M. Star, "Relations between the Kubelka-Munk and the transport equation models for anisotropic scattering," *Lasers Life Sci.* **1**, 287–298 (1987).
68. M. Keijzer, S. L. Jacques, S. A. Prahl, and A. J. Welch, "Light distributions in artery tissue: Monte Carlo simulations for finite-diameter laser beams," *Lasers Surg. Med.* **9**, 148–154 (1989).
69. S. Y. Shchyogolev, "Inverse problems of spectroturbidimetry of biological disperse systems: an overview," *J. Biomed. Opt.* **4**, 490–503 (1999).
70. J. R. Mourant, J. P. Freyer, A. H. Hielscher, A. A. Eick, D. Shen, and T. M. Johnson, "Mechanisms of light scattering from biological cells relevant to noninvasive optical-tissue diagnostics," *Appl. Opt.* **37**, 3586–3593 (1998).

71. J. R. Mourant, T. Fuselier, J. Boyer, T. M. Johnson, and I. J. Bigio, "Predictions and measurements of scattering and absorption over broad wavelength ranges in tissue phantoms," *Appl. Opt.* **36**, 949–957 (1997).
72. R. Graaff, J. G. Aarnoudse, J. R. Zijp, P. M. A. Sloot, F. F. M. de Mul, J. Greve, and M. H. Koelink, "Reduced light-scattering properties for mixtures of spherical particles: a simple approximation derived from Mie calculations," *Appl. Opt.* **31**, 1370–1376 (1992).
73. A. N. Bashkatov, E. A. Genina, V. I. Kochubey, and V. V. Tuchin, "Optical properties of human skin, subcutaneous and mucous tissues in the wavelength range from 400 to 2000 nm," *J. Phys. D* **38**, 2543–2555 (2005).
74. G. Vargas, E. K. Chan, J. K. Barton, and A. J. Welch, "Use of an agent to reduce scattering in skin," *Lasers Surg. Med.* **24**, 133–141 (1999).
75. I. S. Saidi, "Transcutaneous optical measurement of hyperbilirubinemia in neonates," Ph.D. dissertation (Rice University, 1992).
76. S. L. Jacques and D. J. McAuliffe, "The melanosome: threshold temperature for explosive vaporization and internal absorption coefficient during pulsed laser irradiation," *Photochem. Photobiol.* **53**, 769–775 (1991).
77. S. Prahl, "Optical absorption of hemoglobin," <http://omlc.orgi.edu/spectra/hemoglobin/hemestruct/index.html>, accessed 5 Oct. 2009.
78. A. N. Yaroslavsky, A. V. Priezzhev, J. R. I. V. Yaroslavsky, and H. Battarbee, "Optics of blood," in *Handbook of Optical Biomedical Diagnostics*, V. V. Tuchin, ed. (SPIE, 2002), pp. 169–216.
79. S. Wray, M. Cope, D. T. Delpy, J. S. Wyatt, and E. O. Reynolds, "Characterization of the near infrared absorption spectra of cytochrome aa3 and haemoglobin for the non-invasive monitoring of cerebral oxygenation.," *Biochim. Biophys. Acta Bioenerg.* **933**, 184–192 (1988).
80. A. P. Harris, M. J. Sendak, R. T. Donham, M. Thomas, and D. Duncan, "Absorption characteristics of human fetal hemoglobin at wavelengths used in pulse oximetry," *J. Clin. Monitor. Comput.* **4**, 175–177 (1988).
81. S. Takatani and M. D. Graham, "Theoretical analysis of diffuse reflectance from a two-layer tissue model," *IEEE Trans. Biomed. Eng.* **bme-26**, 656–664 (1979).
82. D. W. Marquardt, "An algorithm for least-squares estimation of nonlinear parameters," *J. Soc. Ind. Appl. Math.* **11**, 431–441 (1963).
83. C. Harle-Bachor and P. Boukamp, "Telomerase activity in the regenerative basal layer of the epidermis in human skin and in immortal and carcinoma-derived skin keratinocytes," *Proc. Natl. Acad. Sci. USA* **93**, 6476–6481 (1996).
84. D. Yudovsky, A. Nouvong, K. Schomacker, and L. Pilon, "Two-layer optical model of skin for early, non-invasive detection of wound development on the diabetic foot," *Proc. SPIE* **7555**, 755514 (2010).
85. J. S. Vande Berg and R. Rudolph, "Pressure (decubitus) ulcer: variation in histopathology—a light and electron microscope study," *Hum. Pathol.* **26**, 195–200 (1995).
86. A. J. Boulton, P. Meneses, and W. J. Ennis, "Diabetic foot ulcers: a framework for prevention and care," *Wound Repair Regen.* **7**, 7–16 (1999).